JOURNAL OF MATERIALS SCIENCE 28 (1993) 4412–4420

Banding and the nature of large, irregular pearlite nodules in a hot-rolled low-alloy plate steel: a second report

J. A. ECKERT, P. R. HOWELL
Department of Materials Science and Engineering, The Pennsylvania State University, University Park, PA 16802, USA

S. W. THOMPSON
Advanced Steel Processing and Products Research Center, Department of Metallurgical and Materials Engineering, Colorado School of Mines, Golden, CO 80401, USA

The microstructure of a hot-rolled low-carbon plate steel has been examined using a combination of light microscopy and scanning electron microscopy. It has been found that in the hot-rolled condition, the microstructure consists of alternate bands of ferrite and pearlite, together with relatively large, irregular pearlite nodules. These large nodules were found to be comprised of pearlite, intragranularly nucleated ferrite (both Widmanstätten and idiomorphic), together with carbide-deficient and/or carbide-free regions. It is argued that the carbide-deficient and carbide-free regions form as a result of the premature initiation of the pearlite reaction, i.e. pearlite forms prior to the body of the austenite grains attaining the eutectoid composition. In order to model the formation of the banded structure, specimens were reaustenitized at 1050 °C for 10 min and furnace cooled. This heat-treatment cycle produced an austenite grain size which was less than the chemical banding wavelength. A model for the decomposition of austenite, under these conditions, is presented.

1. Introduction and background

In a recent investigation of a hot-rolled low-alloy plate steel containing 0.15% C [1–4], it was found that the microstructures that developed during the decomposition of austenite could not be rationalized using what might be termed the conventional model of the austenite to ferrite plus pearlite reaction. This model (for example, see [5–8]) involves the formation of a skeleton of ferrite around the austenite grain boundaries. Ferrite growth then continues until the interiors of the austenite grain attain the eutectoid composition; at which point, the pearlite reaction initiates and consumes the remnant parent phase. One obvious consequence of the conventional model is that each austenite grain, upon complete transformation, will yield a single pearlite region consisting of either a single colony or a nodule. In keeping with earlier work [2], we will employ Mehl's definition [9] of a pearlite colony that is ". . . formed as a unit, usually with but one direction of lamellae in which the ferrite and cementite have each a single orientation". It then follows that a nodule is comprised of more than a single colony. What we are terming the conventional model would also imply, at least in low-alloy steels, that pearlitic colonies contain an appreciably constant volume fraction of cementite.

However, as shown by two of the present authors [1, 2], the above model could neither account for the ferrite/pearlite banding, nor for the incidence of large pearlite nodules in a 0.15% C, 1.5% Mn steel. For the sake of completeness, a light micrograph of the 0.15% C, 1.5% Mn steel is shown in Fig. 1. Several ferrite/pearlite bands are arrowed and a number of large pearlite nodules are labelled A. In earlier work [1, 2], models were developed to account for the formation of the microstructures that are illustrated in Fig. 1. In the present study, a different low-alloy steel containing 0.12% C, is examined in order to determine the frequency with which a microstructure, such as that shown in Fig. 1, might be expected to occur. A heat-treatment schedule has also been developed to determine whether or not microstructural banding could occur when the chemical banding wavelength was greater (by a factor of approximately two) than the austenite grain size.

The results of the present study will be compared with those presented elsewhere [1–4].

2. Experimental procedure

The hot-rolled steel, whose composition is given in Table I, was provided by the United States Steel Research Laboratories in Monroeville, PA. The carbon level of this material is somewhat lower than that contained in the alloy which was examined in other work [1–4]. However, the steel employed in the present investigation contains microalloying additions (titanium and vanadium, Table I) which will be im-

0022–2461

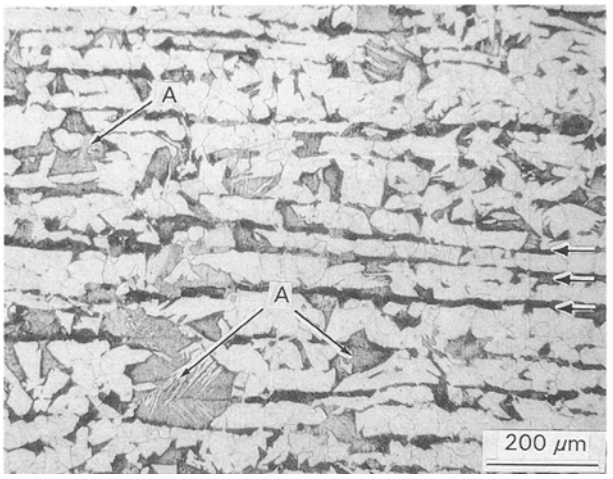

Figure 1 Light micrograph of a 1.5% Mn–0.15% C steel. The microstructure consists of alternate bands of ferrite and pearlite (e.g. arrowed) together with large, irregular pearlite nodules (arrowed A).

TABLE I Chemical composition of the hot-rolled plate (wt %)

C	Mn	Si	P	S	Al	N	Ti	V
0.12	1.53	0.25	0.013	0.002	0.038	0.01	0.016	0.096

portant when the results of the present investigation are compared with previous studies [1, 2].

The steel was hot-rolled at 1200 °C and finish-rolled at ~ 1100 °C. During hot-rolling, the plate thickness was reduced by about 80%. The plate was air-cooled after finish-rolling.

Specimens for light microscopy and scanning electron microscopy were prepared with standard techniques and etched in 2% Nital. The SEM employed was an I.S.I. SX40 operating at 15 kV.

3. Results

3.1. The microstructure of the hot-rolled plate

Fig. 2a and b are low-magnification images of the transverse plane of the plate. In both instances, the microstructures are comprised predominantly of alternate bands of proeutectoid ferrite (the light etching phase) together with pearlite (the dark regions). However, some of the pearlite nodules are not contained within the "pearlite-bands" and several examples are arrowed in Fig. 2a and b. Hence, it can be concluded that the microstructural banding is not a completely accurate reflection of the chemical banding, i.e. the pearlite nodules do not always form in regions of a high manganese content. This is in accord with the discussion presented elsewhere [1] (and see Fig. 1). However, reference to Fig. 1 shows that large nodules occur more frequently and are of a greater size in the 0.15% C alloy as compared with the 0.12% C alloy. Further discussion on this point is deferred to Section 4.

Fig. 3a and b are higher magnification images of the 0.12% C alloy. At these magnifications, the microstructural banding becomes less evident, and the

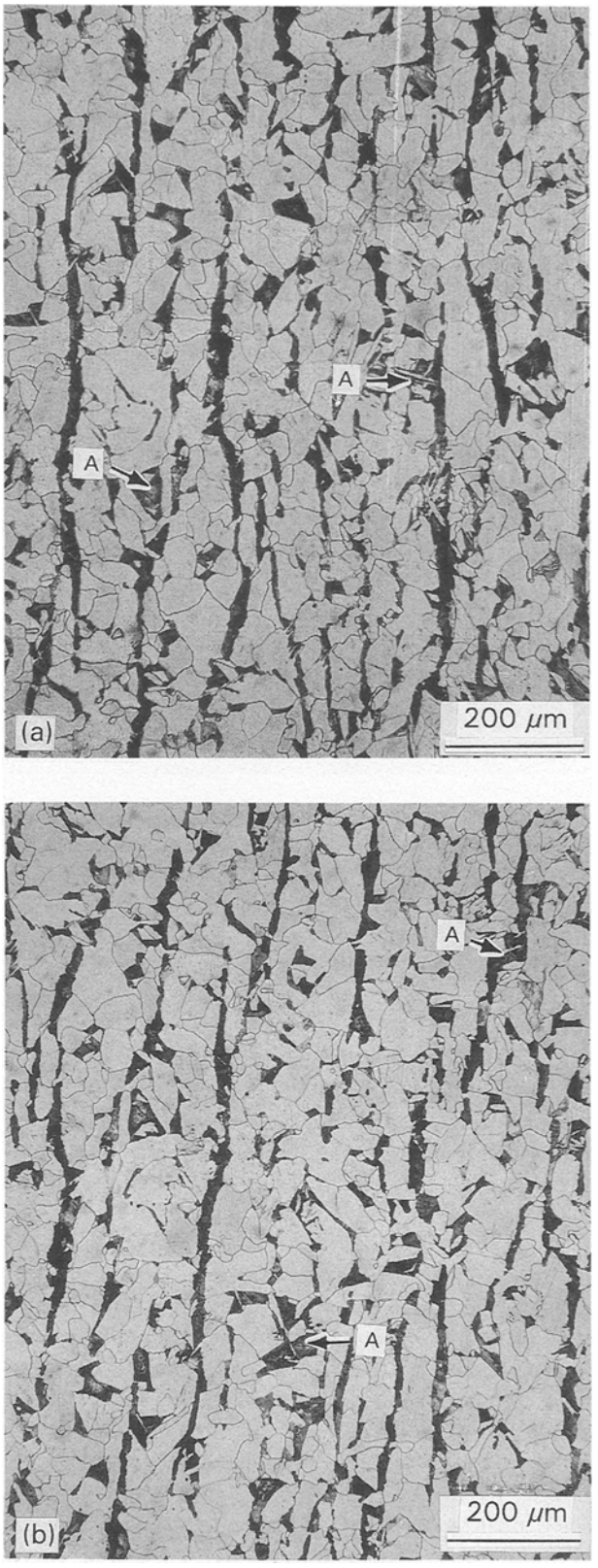

Figure 2 Low-magnification light micrographs of the 1.5% Mn–0.12% C steel. The microstructure again consists of alternate bands of ferrite and pearlite. Some larger nodules have been arrowed, A.

structures of the large irregular nodules become somewhat clearer. Reference to Fig. 3a reveals the presence of nodules ($\simeq 75$ μm diameter) which contain intragranular, idiomorphic ferrite (arrowed A). For comparative purposes, the pearlite nodules which are contained primarily within the bands (e.g. arrowed B in Fig. 3a, b) are ~ 10–20 μm wide. Intragranular

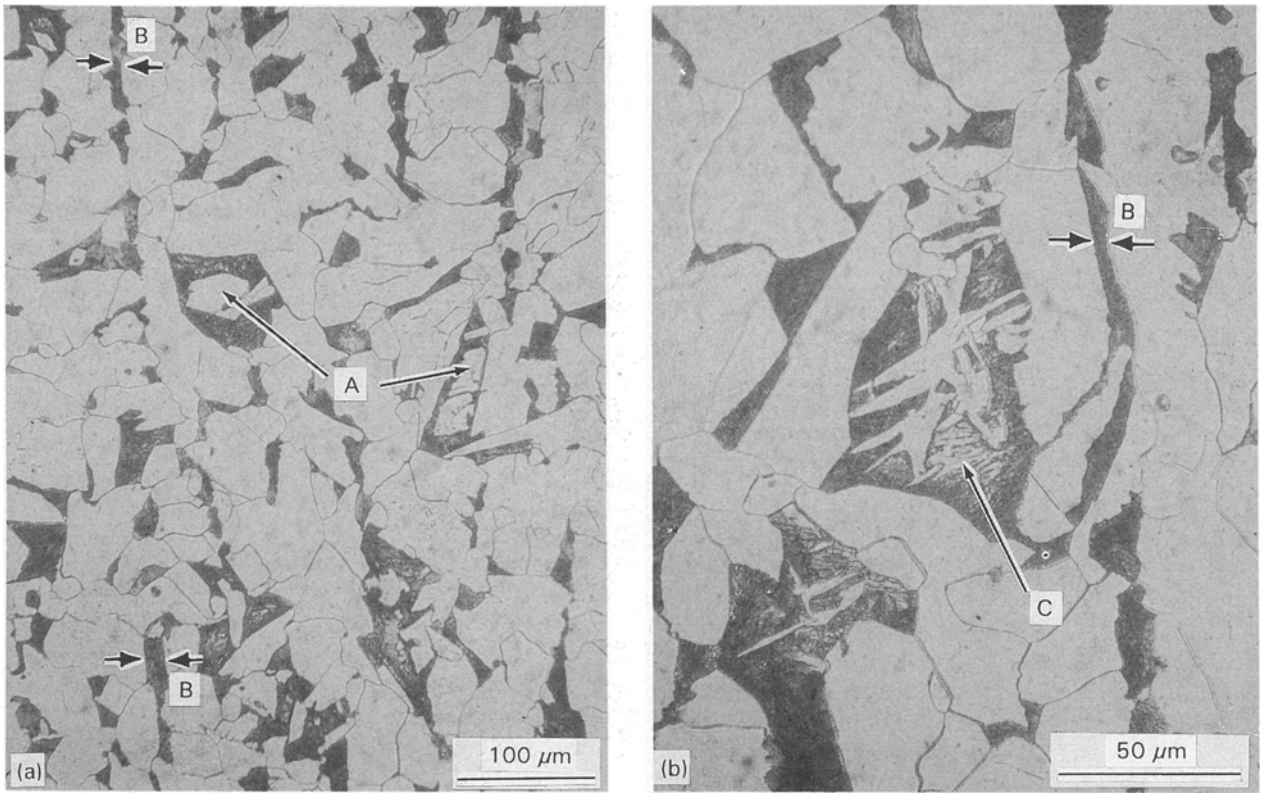

Figure 3 Higher magnification light micrographs of the 0.12 % C steel. (a) Large nodules (~75 μm diameter) in association with idiomorphic ferrite (arrowed A). The widths of the pearlite nodules within the bands (arrowed B) are approximately 10–20 μm. (b) Intragranular Widmanstätten ferrite in association with a large pearlite nodule. Irregularly etching "pearlite" is arrowed, C. The width of the pearlite nodules within the band is indicated at B.

ferrite, primarily Widmanstätten in nature, is also present in the two nodules (approximately 100 μm diameter) in Fig. 3b. Of particular interest in Fig. 3a and b is the irregular etching characteristics of the nodules. For example, the nodules tend to be etched more darkly at their peripheries, but exhibit less uniform etching characteristics within the body of the nodules. This is particularly evident in the nodule towards the centre of the image in Fig. 3b, and is arrowed C. At this point, it can be suggested that, for example, region C on Fig. 3b is a cementite-free or cementite-deficient area within the pearlite nodules.

Fig. 4a and b are SEM images which display features similar to those presented in Fig. 3a and b. (It should be noted that there is a contrast reversal in the SEM; proeutectoid ferrite appears dark and pearlite images as bright regions.) The three large nodules (A–C on Fig. 4a) vary in size from ~40–100 μm and contain numerous intragranularly nucleated ferrite idiomorphs and Widmanstätten plates. The higher magnification image of Fig. 4b serves to illustrate the fact that the cementite in this large irregular nodule tended to be lamellar in nature.

Fig. 5a and b are SEM images of a large nodule which contains cementite-free/deficient regions in the centre of the nodule. The lack of any discernible boundary between these regions (labelled A, Fig. 5a), together with the absence of any well-defined morphology implies that:

(i) these predominantly ferritic regions are not intragranularly nucleated; but

(ii) they form in association with the "austenite to pearlite" reaction.

Supportive evidence for this contention is provided in Fig. 5b where an almost cyclic formation of irregular ferrite/cementite aggregates has developed (arrowed) in association with cementite-free areas, to yield the overall cementite-deficient region.

A further example of cementite-deficient regions is presented in Fig. 6. However, in this instance, the carbide-depleted zones occur both towards the centres of the nodule (A) and towards its periphery (arrowed B). The implications of this latter observation will be discussed in Section 4. Finally, Fig. 7 is included to justify the term nodule, at least six different colonies (A–F) are seen to constitute this entity.

3.2. Microstructural banding in a reaustenitized and furnace-cooled sample

Fig. 8a and b are light micrographs of specimen material which had been reaustenitized at 1050 °C for 10 min and furnace cooled. Reference to these figures shows virtually perfect microstructural banding and no large, irregular pearlite nodules. To facilitate further discussion, the banding wavelength was determined to be close to 100 μm and the volume fraction of pearlite in the furnace-cooled material was ~ 12%. The austenite grain size after 10 min at 1050 °C was determined to be 50–55 μm with a relatively narrow

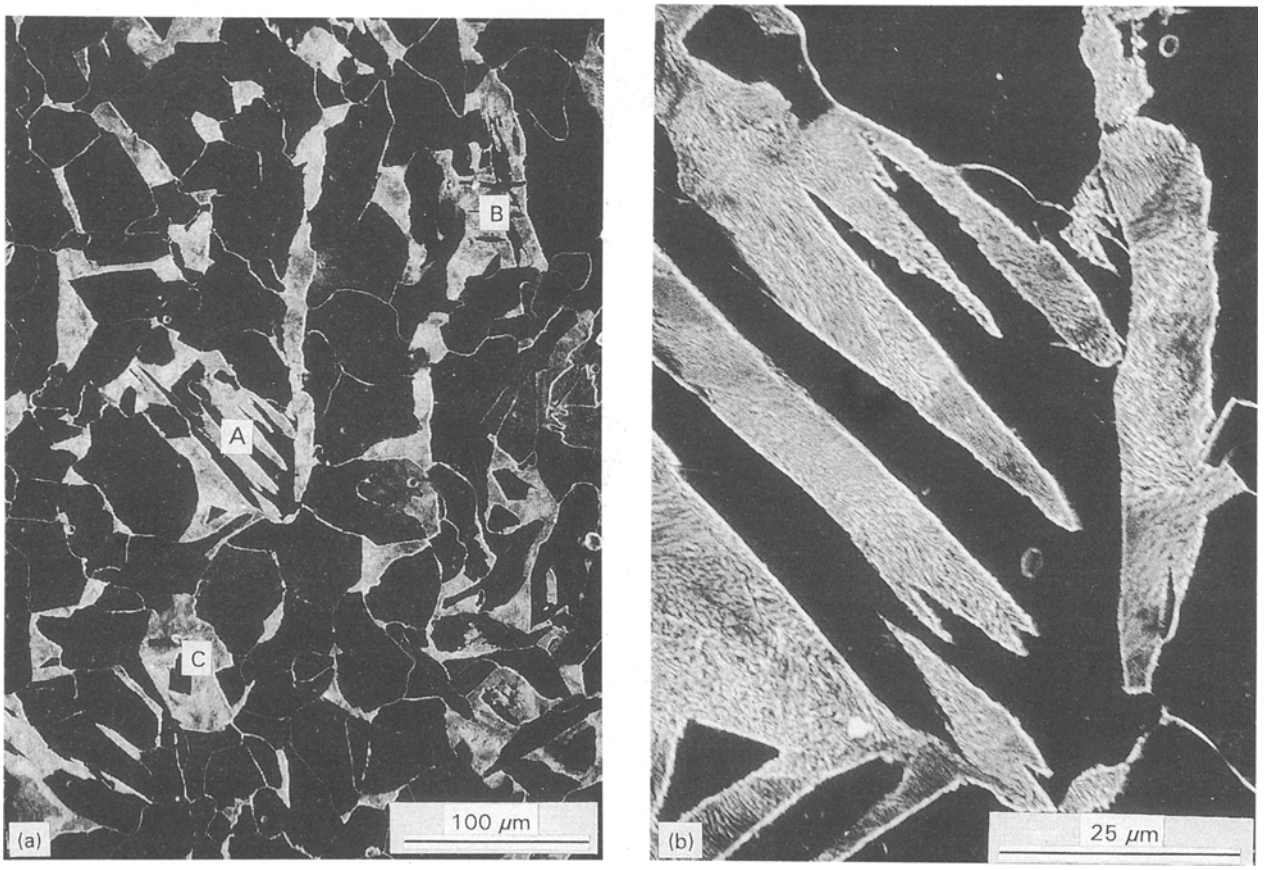

Figure 4 Scanning electron micrographs images. Note the contrast reversal with respect to Figs 1–3. (a) Low-magnification image. Three nodules (A–C) contain intragranular Widmanstätten ferrite. (b) High-magnification image of nodule A. The cementite is seen to be predominantly lamellar.

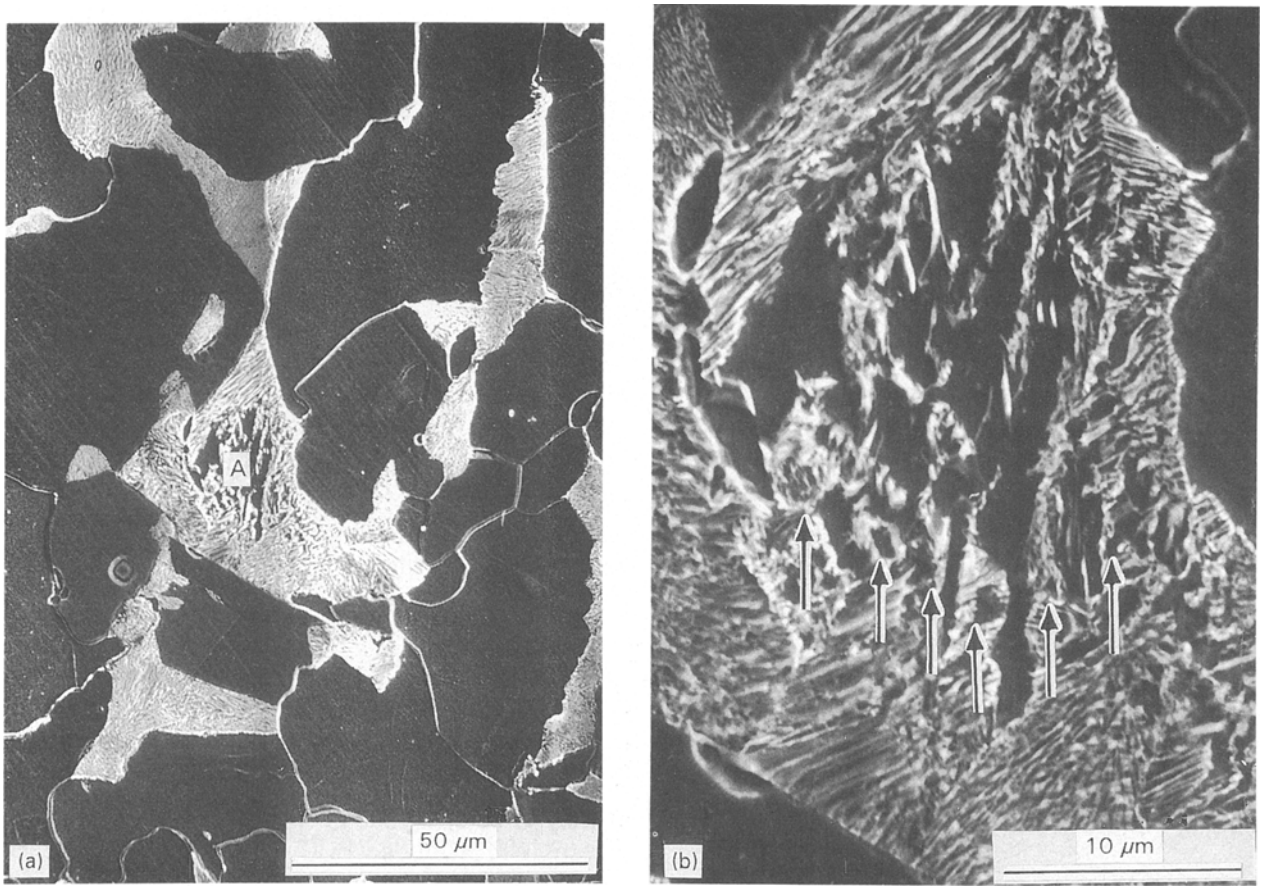

Figure 5 Scanning electron micrographs of a single nodule. (a) A cementite-deficient region (A) is located towards the centre of the nodule. (b) Higher magnification image showing almost cyclic formation of cementite-free regions.

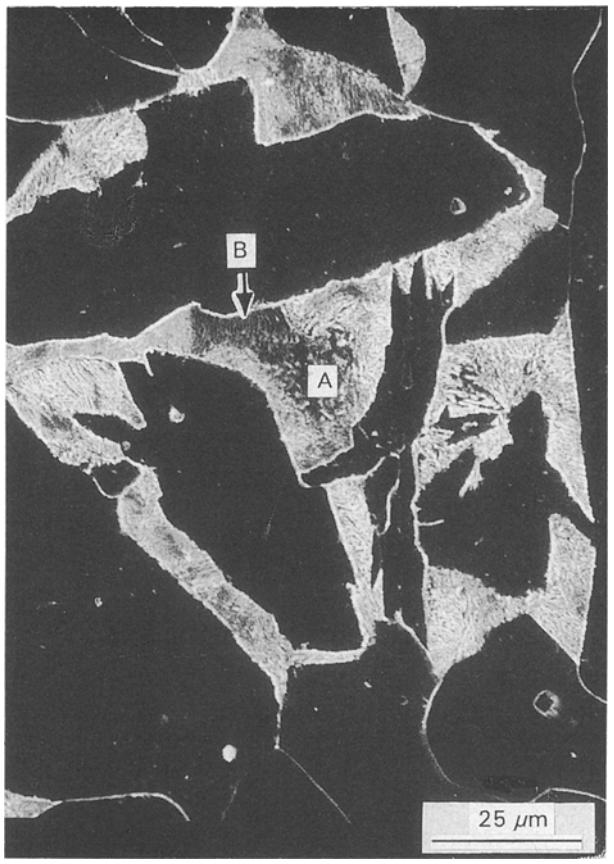

Figure 6 Scanning electron micrograph of a complex nodule. Cementite deficient regions are present, both towards the centre of the nodule (A) and towards the periphery (B).

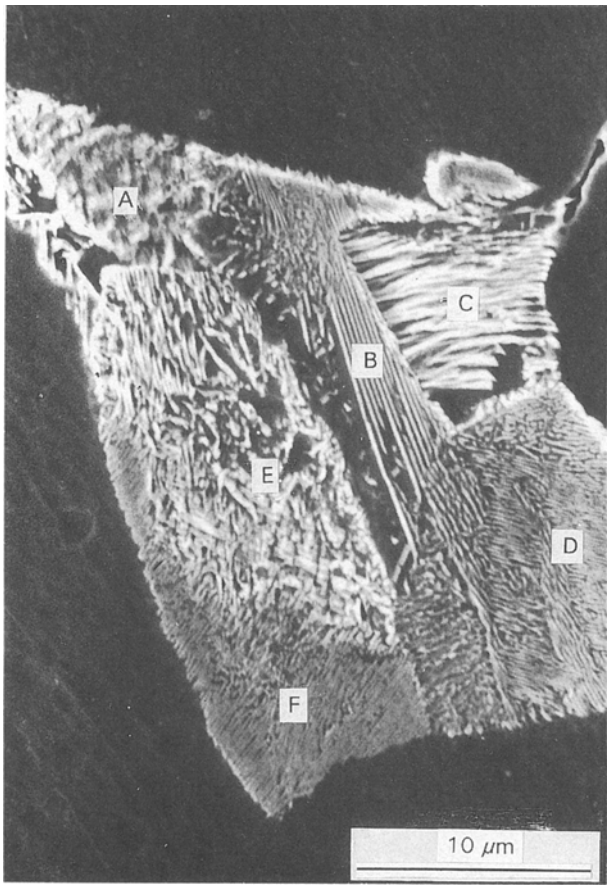

Figure 7 A pearlite nodule which is comprised of at least six pearlite colonies (A–F).

distribution, the largest austenite grains being 80–100 μm diameter.

4. Discussion

4.1. The nature and origin of the large irregular pearlite nodules

The observation of relatively large, irregular pearlite nodules is in agreement with the earlier studies of two of the present authors [1, 2] who examined a 0.15% C – 1.5% Mn steel. However, a comparison of Fig. 1 with Figs 2–7 reveals that the nodules which were found in the present study were small (size range 30–100 μm) as compared with those in the 0.15% C steel (size range up to 200 μm, e.g. see Fig. 1). This difference is most likely due to differences in austenite grain size; the microalloying additions in the present system, acting to retard grain growth. This is substantiated by the fact that even after 10 min at 1050 °C, the average grain size was only 50 μm with a maximum size of about 100 μm. Conversely, for the 0.15% C steel, grains as large as 100 μm were found after 10 min at 900 °C. In other respects, the nodules which have been investigated in the present study bear a marked resemblance to those in the 0.15% C steel in that:

(i) many of the nodules contain intragranularly nucleated ferrite (both Widmanstätten and idiomorphic);

(ii) many of the nodules contain cementite-free or cementite-deficient regions.

The observation of intragranular ferrite in the large nodules implies that the large nodules form from the larger austenite grains. This follows because diffusion distances are longer and a substantial carbon build-up in the grain interiors will be time-consuming, thereby permitting intragranular ferrite nucleation [10]. Conversely, in small austenite grains, rapid carbon enrichment of the austenite grain centres will seriously inhibit the nucleation of ferrite.

The observation of cementite-free and cementite-deficient regions, often towards the centres of the pearlite nodules, can be explained if the pearlite reaction is initiated, well before the entire austenite grain has attained the eutectoid composition. The following is a modified and condensed version of the discussion presented elsewhere [2]. However, it is considered that this discussion is mandatory if the results of this paper are to be adequately explained. Fig. 9a is a schematic drawing of the free-energy/composition curves for a temperature at which the stable phases are ferrite, α, and cementite, Fe_3C. Although the argument is then for an isothermal transformation, we believe that the resultant hypotheses should be applicable also to continuous cooling transformations. If the metastable equilibria between α (composition x_1) and γ (composition x_3), and between Fe_3C (composition x_4) and γ (composition x_2) are considered, then at time $t = 0$, an alloy of composition x_0 will be supersaturated with respect to α but not with respect to Fe_3C. Hence, proeutectoid ferrite will be the first phase to form. During growth of this proeutectoid α, a diffusion profile will develop in the austenite ahead of the

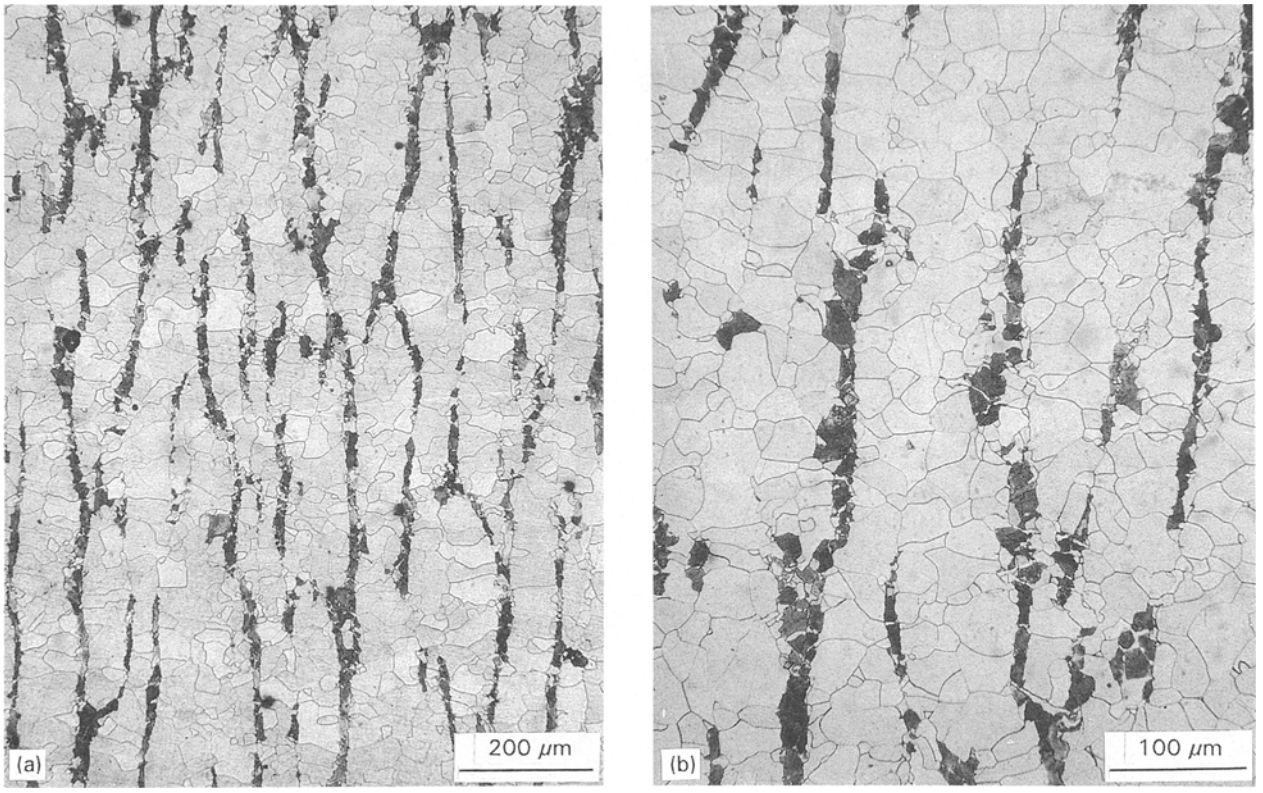

Figure 8 Light micrographs of specimen material which had been reaustenitized and furnace cooled. Almost perfect microstructural banding is observed. Many of the ferrite grains are columnar.

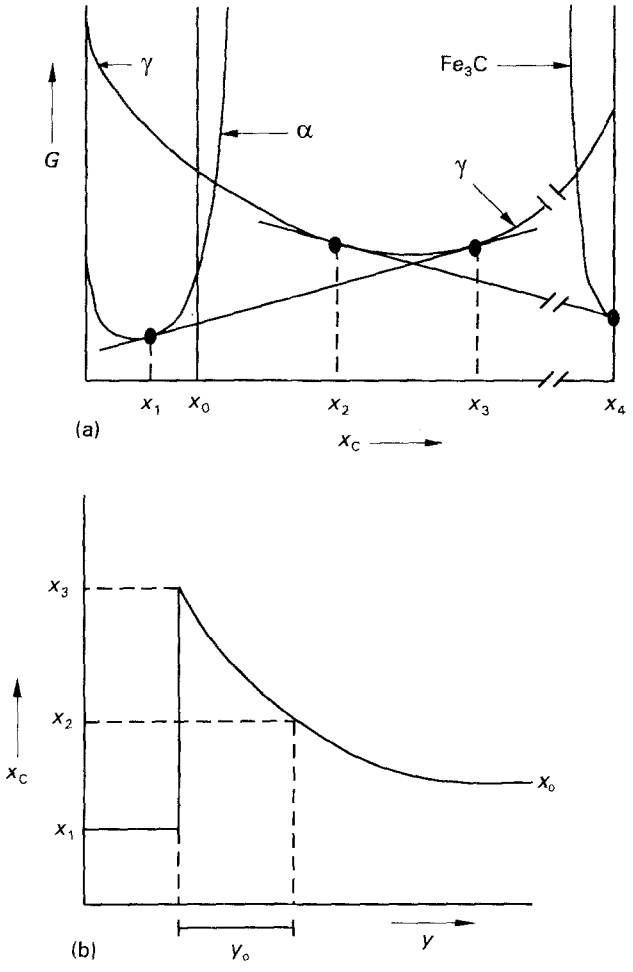

Figure 9 Equilibrium between austenite, γ, ferrite, α and cementite in the two-phase (α + Fe_3C) region. (a) Free-energy/composition curves defining the metastable equilibria between γ and α and between γ and Fe_3C (for details, see text). (b) Diffusion profile in the vicinity of the γ/α interface (see text for details).

growing α; this profile is shown in Fig. 9b. Now, if it is assumed that there is local equilibrium at the α/γ interface (i.e. the γ → α reaction is occurring under full diffusion control), then a zone of width y_0 in front of the interface is supersaturated with respect to both ferrite and cementite. This latter point can be appreciated by referring to the free-energy curves of Fig. 9a, which predicts that as soon as the austenite composition reaches x_2, it is supersaturated with respect to cementite as well as ferrite.

Therefore, we are suggesting that when the width of the supersaturated zone reaches some critical value, cementite nucleates on the γ/α interface and the pearlite reaction is initiated. However, the pearlite reaction cannot be sustained for the entire transformation, because regions which are remote from the pearlite initiation sites have compositions at, or close to x_0 (e.g. see Fig. 9b). Hence, as the pearlite colonies/nodules "move through" the diffusion profiles in the austenite interiors, they encounter regions of lower carbon concentrations and the supersaturated zone will become narrower and narrower. Hence, the pearlite reaction may terminate eventually to be replaced by the proeutectoid ferrite reaction. Now, during growth of the ferrite, the supersaturated zone will again increase in width and the pearlite reaction may again be initiated. Hence, we envisage a cyclic process for the formation of pearlite and proeutectoid ferrite. This hypothetical sequence of events is in good agreement with the experimental images of, for example, Fig. 5a and b where the alignment of pearlitic and proeutectoid ferritic regions is particularly evident. Our hypothesis is also consistent with the carbide-free/carbide-deficient regions being located frequently towards the centres of the large pearlite nodules.

However, it was not unusual to find cementite-deficient regions towards the periphery of the pearlite nodules (Fig. 6). This may be explained as follows. It is well known that many proeutectoid ferrite/austenite interfaces do not initiate the pearlite reaction (for example, see [11, 12]) and this leads eventually to the formation of impingement interfaces between pearlitic ferritic and proeutectoid ferrite. A natural consequence of this phenomenon will be the formation of carbide-free regions in the vicinity of impingement interfaces. This may be explained with reference to the schematic drawings of Fig. 10. In Fig. 10a, it is assumed that a single pearlite colony, which constitutes part of a nodule, has advanced to a sufficient extent that carbide-free regions (i.e. proeutectoid ferrite, α_1) is forming. Hence, there is a relatively narrow diffusion profile ahead of the advancing interface (Fig. 10b). Now, suppose that there is a proeutectoid grain (α_2 in Fig. 10a) that will not initiate the pearlite reaction; rather, it will form an impingement interface with α_1. During continued growth, the diffusion profile which is associated with α_1 will increase in width and eventually overlap that of the proeutectoid grain α_2, thus yielding a microstructure and concentration profile similar to that shown in Fig. 10c and d, respectively. At some point, the remaining austenite must be sufficiently supersaturated with respect to carbon, that nucleation of cementite occurs on the α_1/γ interface (we are still assuming that the α_2/γ interface cannot initiate the pearlite reaction). Now, depending on the

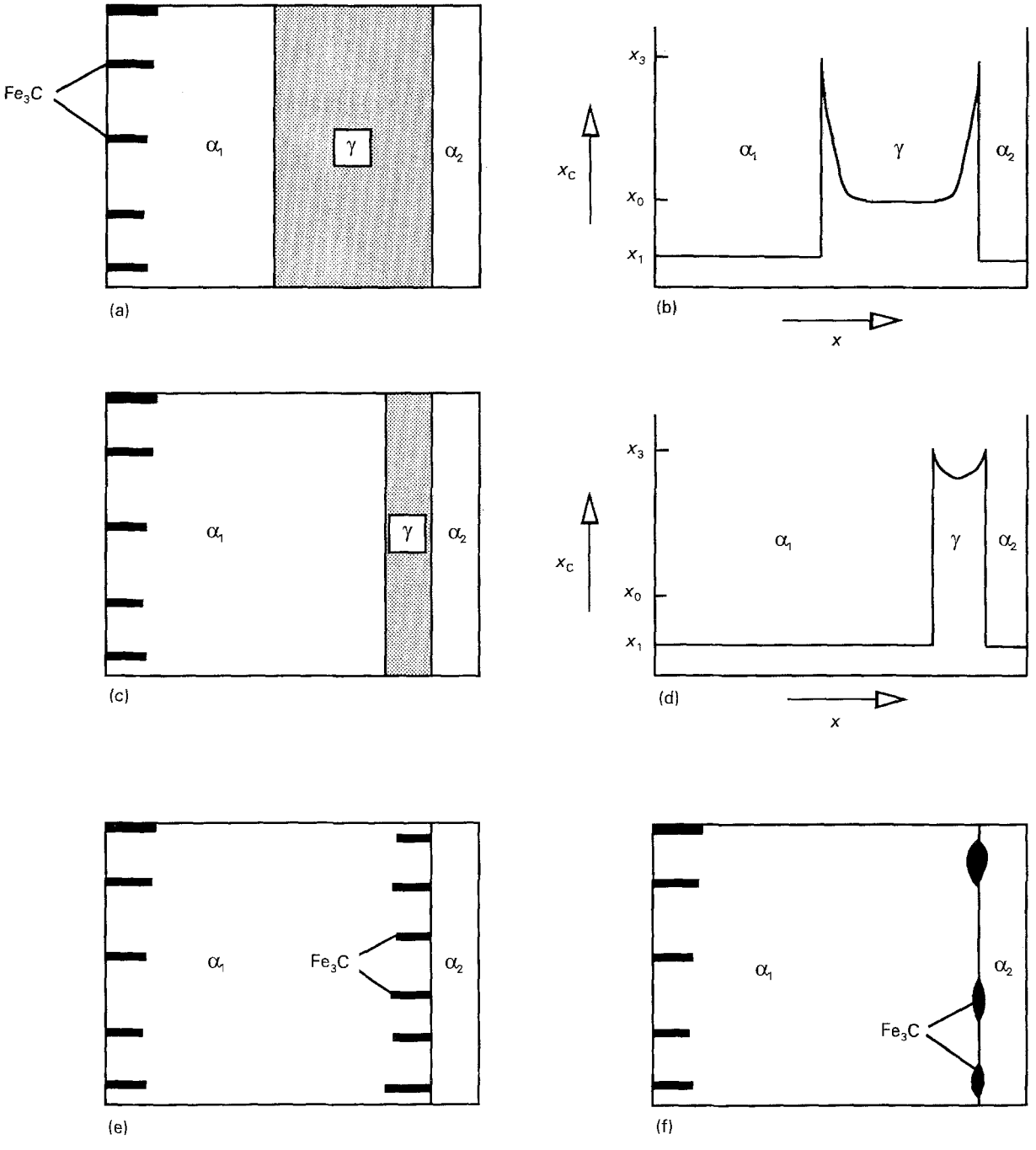

Figure 10 Schematic diagrams illustrating the formation of either pearlite or grain-boundary carbides at impingement interface (for details, see text). (a) Cementite-free ferrite, α_1 and a proeutectoid ferrite grain, α_2. (b) Possible carbon concentration profile for (a). (c) As for (a), but after further growth of α_1 has occurred. (d) Possible carbon concentration profile for (c). (e) Decomposition of the remnant austenite in (c) to pearlite. (f) Alternative mode of decomposition to yield grain-boundary cementite.

width of the austenite which remains to be transformed, pearlite or grain-boundary carbides can form. Fig. 10e shows the formation of pearlite from a "relatively" wide zone of austenite. In comparison, Fig. 10f shows a possible transformation mode when the width of the latterly transforming region is narrow enough, that cooperation [13] cannot be attained and multiple nucleation of cementite on the α_1/γ interface drains the remnant austenite in carbon. This will favour growth of α_2 and the formation of grain-boundary cementite.

At this point it would be noted that:

(i) the model predicts that carbides (whether discrete or as lamellae) should always be present at the periphery of the nodules. This is indeed the case for the image shown in Fig. 6 where the carbide deficient region formed towards the periphery of the nodules;

(ii) the same model can be applied for the case of two carbide-deficient regions within a pearlite nodule. Hence, it is also predicted that grain boundaries in pearlite nodules should always be associated with cementite. A transmission electron microscopy study of the 0.15% C steel [2] has indeed shown this to be the case.

4.2. The development of banded and non-banded microstructures

In this section, the formation of a perfectly banded microstructure in the furnace cooled samples will be modelled. This will be followed by a discussion of the lack of microstructural banding within the large, irregular nodules in the as-received air-cooled samples.

Reference to Fig. 8a and b shows that almost perfect microstructural banding develops upon slow cooling from the austenite range. This is of particular interest in that the microstructural, and hence chemical, banding wavelength is $\sim 100\ \mu m$, whereas the ferrite/pearlite bands are forming from austenite grains with an average size of 50–55 μm (Thompson and Howell [1] have shown that there is a one-to-one correlation between the regions of high manganese and the pearlite bands in furnace-cooled samples). Fig. 11 is a schematic drawing of the early stages of the decomposition of austenite during slow cooling. Fig. 11 is drawn to scale and the 12%–15% of austenite that will transform eventually to pearlite is between the closely spaced parallel bands. Because manganese is an austenite stabilizer, it serves to depress the Ar_3 temperature. Hence, it is assumed that the first-formed proeutectoid ferrite is located towards the centre of the manganese lean regions, on grain-boundary quadruple points and triple junctions. Preferential growth of this proeutectoid ferrite along grain boundaries, again located towards the centres of the manganese-rich regions, will eventually lead to a "slab of ferrite" which is approximately parallel to the austenitic regions that will transform eventually to pearlite. Once the ferritic slab has formed, growth can only continue in a direction towards the manganese-rich regions. This growth will be accompanied by the diffusion of carbon towards the manganese-rich regions. Finally, the pearlite reaction will be initiated and a perfectly banded microstructure will result.

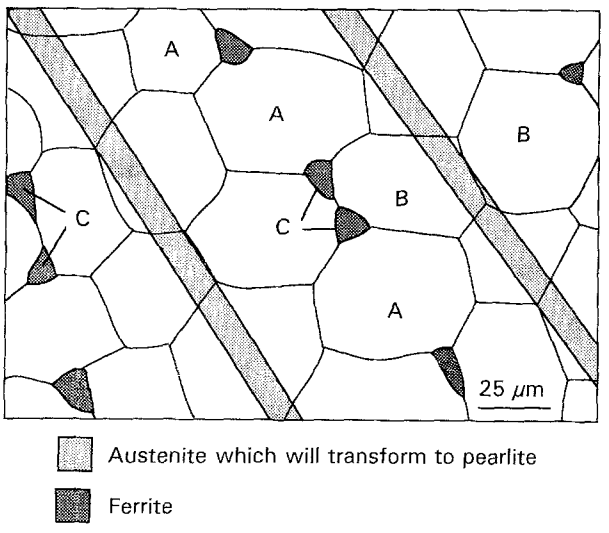

Figure 11 A schematic scale drawing of the early stages of the ferrite reaction. The shaded bands are assumed to be the high manganese regions which will eventually transform to austenite. Hence, ferrite nucleation (e.g. arrowed C) occurs in the manganese-lean regions (see text for details).

Some interesting consequences of this model are as follows:

(i) ferrite must be able to grow through austenite triple junctions in order to form the "ferritic slab";

(ii) growth of the ferritic slab towards the manganese-rich regions should favour the formation of columnar ferrite grains. This indeed is the case as is evident in Fig. 8b;

(iii) entire grains of austenite (e.g. labelled A, Fig. 11) must transform to 100 % ferrite. Others (labelled B) must transform predominantly to ferrite.

Now, reference to Fig. 2a and b (the as-received air-cooled samples) shows that microstructural banding is not as severe for cooling rates ($\simeq 1\,^{\circ}C\,s^{-1}$) in excess of those experienced for furnace-cooled samples ($\sim 0.1\,^{\circ}C\,s^{-1}$). This is not unreasonable in that the more rapid cooling will yield higher driving forces for the ferrite reaction, and differences in the Ar_3 temperatures between the manganese-lean and manganese-rich regions, should have a lesser effect. This is also consistent with a discussion presented by Samuels [14]. A consequence of the above is that there is some critical cooling rate, above which microstructural banding will no longer be evident. In the present study and for the given grain size, this cooling rate is between 1 and $5\,^{\circ}C\,s^{-1}$, because the latter cooling rate (generated by a rapid air cool) yielded a non-banded structure.

Reference to Fig. 2a and b shows that the large pearlite nodules occur in both ferrite and pearlite bands. Furthermore, reference to Figs 3–8 shows that the chemical banding has no discernible effect on the microstructure of the nodules. Hence, for the decomposition of the large austenite grains, we are already above the critical cooling rate for microstructural banding. This is not unreasonable in that the potency of grain boundaries as nucleation catalysts, will far outweigh any variation in the Ar_3 temperature.

5. Conclusions

The microstructure of a hot-rolled low-carbon (0.12%) steel consists of alternate bands of proeutectoid ferrite and pearlite, together with large, irregular pearlite nodules. These latter entities consist of multiple pearlite colonies, intragranular ferrite (both Widmanstätten and idiomorphic), and carbide-deficient carbide-free regions. These latter ferritic areas form in association with the pearlite reaction. It is considered that pearlite can be initiated well before the entire austenite grain attains the composition which is given by the Hultgren extrapolation. This leads to the cyclic formation of pearlite and cementite-free regions.

A microstructural investigation of specimen material which had been reaustenitized and subsequently furnace-cooled, has led to the development of a new model for the decomposition of austenite in chemically banded steels. The model involves nucleation of ferrite in solute-lean regions as originally described elsewhere [1], the subsequent formation of "ferrite slabs" and the transformation of entire grains of austenite, to ferrite.

References

1. S. W. THOMPSON, PhD thesis, The Pennsylvania State University, PA (1986).
2. S. W. THOMPSON and P. R. HOWELL, *Mater. Sci. Technol.*, in press.
3. *Idem, ibid.*, submitted.
4. *Idem, ibid.*, submitted.
5. D. R. ASKELAND, "The Science and Engineering of Materials" (Brooks/Cole Engineering Division, Monterey, CA, 1984) p. 293.
6. R. E. REED HILL and R. ABBASCHIAN, "Physical Metallurgy Principles", 3rd Edn. (P.W.S. – Kent, Boston, MA, 1992) p. 623.
7. W. F. SMITH, "Principles of Materials Science and Engineering" (McGraw-Hill, London, 1986) p. 447.
8. P. G. SHEWMAN, "Transformations in Metals" (McGraw-Hill, London, 1969) p. 234.
9. R. F. MEHL, *JISI* **159** (1948) 113.
10. H. I. AARONSON, in "Decomposition of Austenite by Diffusional Processes", edited by V. F. Zackay and H. I. Aaronson (Interscience, New York, 1962) p. 387.
11. J.-W. LEE and P. R. HOWELL, *J. Mater. Sci.* **22** (1987) 3631.
12. J-W. LEE, S. W. THOMPSON and P. R. HOWELL, *ibid.* **25** (1990) 1699.
13. M. HILLERT, in "Decomposition of Austenite by Diffusional Processes", edited by V. F. Zackay and H. I. Aaronson (Interscience, New York, 1962) p. 289.
14. L. E. SAMUELS, "Optical Microscopy of Carbon Steels" (ASM, Metals Park, OH, 1980) p. 127.

Received 10 March 1992
and accepted 15 January 1993